Nonorthogonal object identification based on ghost imaging

Xiaofan Gu[1] and Shengmei Zhao[1,2,*]

[1]*Institute of Signal Processing & Transmission, Nanjing University of Posts and Telecommunications (NUPT), Nanjing 210003, China*

[2]*Key Lab of Broadband Wireless Communication and Sensor Network Technology, NUPT, Ministry of Education, Nanjing 210003, China*

**Corresponding author: zhaosm@njupt.edu.cn*

Received May 11, 2015; revised July 21, 2015; accepted July 22, 2015;
posted July 23, 2015 (Doc. ID 240028); published August 24, 2015

Ghost imaging could be used to make a quick identification of orthogonal objects by means of photocurrent correlation measurements. In this paper, we extend the method to identify nonorthogonal objects. In the method, an object is illuminated by one photon from an entangled pair, and the other one is diffracted into a particular direction by a pre-established multiple-exposure hologram in the idler arm. By the correlation measurements, the nonorthogonal object in the signal arm could be discriminated within a very short time. The constraints for the identification of nonorthogonal objects are presented, which show that the nonorthogonal objects can be discriminated when the overlapping portion between any two objects is less than half of all the objects in the set. The numerical simulations further verify the result.

OCIS codes: (110.2970) Image detection systems; (270.5585) Quantum information and processing.
http://dx.doi.org/10.1364/PRJ.3.000238

1. INTRODUCTION

Object identification can be described as discriminating one object from a set of objects according to some unique characteristics, and it has extensive applications in visual learning and object tracking [1,2]. Several technologies are available to make object identification, but they all have limitations. Barcode is a commonly used identification method today, but it requires reading devices and tags, and often does not work without human intervention [3]. Radio frequency identification (RFID) is a popular and representative technique, but mostly for identifying the individual objects [3].

Most of the existing object identification methods are required to get the object first, but sometimes it is hard to reach the object. In other words, identification should be accomplished without directly acquiring the object's information. Ghost imaging [4,5], which is also known as two-photon imaging or correlated imaging, can be suitable for this case to make object identification. In 2010, Malik *et al.* proposed a method based on ghost imaging to discriminate orthogonal objects with little photons and a short processing time [6]. However, it does not work on overlapping objects.

In a ghost imaging system, there are generally two light beams [4,5]. One beam, named the signal beam, passes through an object and is collected by a bucket detector. The other beam, named the idler beam, is detected by a spatially resolving detector. A high-resolution image could be obtained in the idler arm by coincidence counting the two detectors.

The first ghost imaging scheme based on entangled photon pairs was demonstrated by experiments in 1995 [7]. Later, classical light sources, especially pseudo-thermal sources, were used to implement the experiments [8]. Both the entangled sources and the thermal light sources can be used to realize ghost imaging [9–16], and the comparison between the two sources has been discussed. With the application of a spatial light modulator (SLM), a computational ghost imaging scheme [17] and a single detector ghost imaging scheme [18] turned out, and made it more mature and easier to implement a ghost imaging system.

In this paper, we extend the identification method based on ghost imaging for the nonorthogonal objects. In the method, an unknown object is illustrated by the signal photons, and simultaneously the idler photons are diffracted into a particular direction by a pre-established multiple-exposure hologram set after the ghost imaging position. By the correlation measurement between the signal photons and idler photons, the nonorthogonal objects in the signal arm could be discriminated in a very short processing time.

The remainder of this paper is as follows. The method for nonorthogonal object identification is presented in Section 2. The numerical simulations are given in Section 3. The conclusions are drawn in Section 4.

2. SCHEME FOR NONORTHOGONAL OBJECT IDENTIFICATION BASED ON GHOST IMAGING

The schematic diagram of nonorthogonal object identification based on ghost imaging is shown in Fig. 1. A pump source is focused on a BBO crystal to produce entangled photon pairs and then separated into two beams, named the signal beam and the idler beam. The signal beam illuminates an object for identification and then is collected by a following bucket detector D_1. The idler beam illuminates the pre-established multiple-exposure hologram, which is made by nonorthogonal objects, and then is diffracted into a certain direction corresponding to the object in the signal arm. Each output beam from the hologram is collected by a certain detector, such

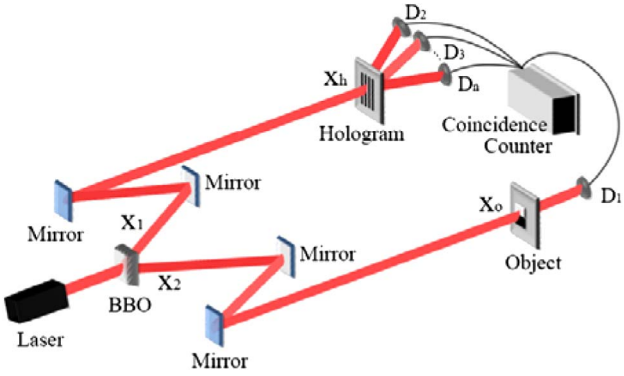

Fig. 1. Schematic setup of quantum ghost image identification with correlated photon pairs.

as D_2, $D_3 \ldots D_n$. By the coincidence counting between signal detector D_1 and detectors in different directions, the object placed in the signal arm can be discriminated from a set of objects without directly acquiring any spatial information about it. Considering the case of two nonorthogonal objects, the coincidence counting results of the two detectors can be generally expressed as follows:

$$C = \int \mathrm{d}x_i \mathrm{d}x_s \mathrm{d}x_o \mathrm{d}x_h |f(x_i, x_h) f(x_s, x_o) T(x_o) \times H(x_h) \psi(x_i, x_s)|^2, \quad (1)$$

where x_i and x_s denote the positions at the SPDC plane, and x_o and x_h denote the positions at the object plane and hologram plane, respectively. $\psi(x_i, x_s)$ describes the process of SPDC, which can be approximated as $\psi(x_i, x_s) \propto \delta(x_i, x_s)$. $f(x_1, x_2)$ is a weighting function describing the propagation from position x_1 to x_2, which can be written as $f(x_1, x_2) = \frac{2^{1/4}}{\sqrt{\pi\omega\sigma}} e^{-(x_1+x_2)^2/4\omega^2} e^{-(x_1-x_2)^2/2\sigma^2}$. $T(x_o)$ is the transmission function of a certain object, and $H(x_h)$ is a transmission function of the multiple-exposure hologram established from a set of nonorthogonal objects.

The pre-established multiple-exposure hologram is a key component of the whole system, which is produced by interfering the object beam with the reference beam, repeatedly. A set of nonorthogonal objects, which determines the range of identification, is used to generate object beams. Also, it is noted that the directions of the reference beams are different corresponding to different object beams. The procedure of establishing the hologram is shown in Fig. 2.

Importantly, the hologram is object-specific. All the objects, which could be identified, should be stored in the hologram before using this system to identify a certain object.

When a light beam carrying the same object information illuminates on the established hologram, the output beam is diffracted into a certain direction, depending upon the corresponding reference beam used in the establishing procedure. As a result, the object can be discriminated by detecting the directions of the output beams. This procedure is shown in Fig. 3.

The local optical intensity I of the n-times-exposure hologram can be expressed as the sum of the intensity of each exposure,

$$I = |O(x)t_1(x) + R_1(x)|^2 + |O(x)t_2(x) + R_2(x)|^2 \ldots + |O(x)t_n(x) + R_n(x)|^2, \quad (2)$$

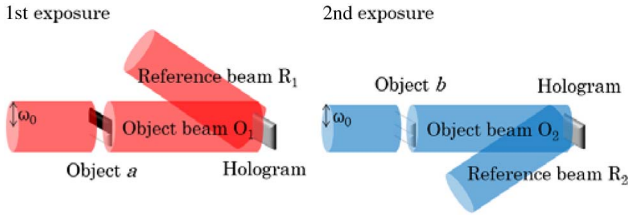

Fig. 2. Procedure for establishing a two-times-exposure hologram. A light beam carrying the information of object a, denoted as object beam O_1, first interferes with the reference beam R_1 on the hologram. Then, another light beam carrying the information of object b, denoted as object beam O_2, interferes with another reference beam R_2 on the same hologram. So, the established two-times-exposure hologram contains the information of both object a and object b.

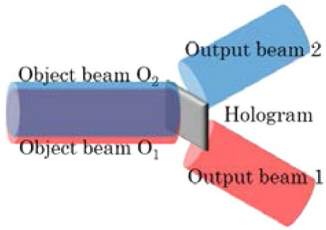

Fig. 3. Procedure of object discrimination using the multiple-exposure hologram. The information of object a and object b is already stored in the hologram. When the light beam carrying the information of object a, denoted as object beam O_1, illuminates the hologram, the output beam is diffracted into the direction the same as the direction of the reference beam R_1 in the hologram establishing procedure. The same result is applicable to object b.

where $O(x)$ denotes the original light beam used to generate the object beam. $R_i(x)$ and $t_i(x)$ denote the reference beam and the transmission function of the nonorthogonal object used in the ith exposure, respectively.

It is assumed that the transmission $H(x)$ of the hologram is proportional to the local optical intensity I; that is

$$H(x) \propto |O(x)t_1(x) + R_1(x)|^2 + |O(x)t_2(x) + R_2(x)|^2 \ldots + |O(x)t_n(x) + R_n(x)|^2. \quad (3)$$

So, when the hologram is illuminated by a replica of the object beam (such as $O(x)t_1(x)$), the output beam through the hologram can be expressed as

$$\begin{aligned} E_{\mathrm{out}} &\propto Ot_1(x)H(x) \\ &\propto (t_1^3(x)|O|^2 + t_1(x)|R|^2)O + t_1^2(x)O^2R_1^* \\ &\quad + t_1^2(x)|O|^2R_1 + (t_1(x)t_2^2(x)|O|^2 + t_1(x)|R_2|^2)O \\ &\quad + t_1(x)t_2(x)O^2R_2^* + t_1(x)t_2(x)|O|^2R_2 \\ &\quad + \ldots + (t_1(x)t_n^2(x)|O|^2 + t_1(x)|R_n|^2)O \\ &\quad + t_1(x)t_n(x)O^2R_n^* + t_1(x)t_n(x)|O|^2R_n. \end{aligned} \quad (4)$$

Each term in Eq. (4) is a potential output of photons. It is seen that each term containing R_n is the one leading to diffract the output beam in the R_n direction. So, the $H(x)$ of the hologram can be simply expressed as

$$H(x) \propto t_i(x) \quad \text{in } R_i \text{ derection.} \quad (5)$$

When the beam radius ω is very large and the transverse coherence length σ is very small in comparison with the size

of the binary amplitude objects, the joint detection probabilities of the two directions can be expressed as

$$C \propto |\int \mathrm{d}x_o t_a(x_o) t_b(x_o)|^2 , \tag{6}$$

$$C \propto |\int \mathrm{d}x_o t_a^2(x_o)|^2 . \tag{7}$$

So, Eq. (6) gives the probability of the coincidence result being recorded between detector D_1 and the detector that is not corresponding to the object in the signal arm. Equation (7) gives the probability of the coincidence result being recorded between detector D_1 and the detector that is corresponding to the object in the signal arm.

The inner product $\int \mathrm{d}x_o t_a(x_o) t_b(x_o)$ of the two objects' transmission functions determines whether the objects are orthogonal. For the orthogonal objects, the inner product is zero, so the value of Eq. (6) is always 0. But for the nonorthogonal objects, the inner product $\int \mathrm{d}x_o t_a(x_o) t_b(x_o)$ is nonzero; hence, the value of Eq. (6) is not 0 anymore. In order to discriminate the two nonorthogonal objects, distinct differences between Eqs. (6) and (7) should be made.

We assume that the largest overlap for any two nonorthogonal objects is 1/2. It is shown that the coincidence ratio of Eq. (7) over Eq. (6) is M^2 if the overlap for objects a and b is 1/M. Hence, when the value of Eq. (7) is four times larger than the value of Eq. (6), it is possible to discriminate the two nonorthogonal objects. That is,

$$4\left|\int \mathrm{d}x_o t_a(x_o) t_b(x_o)\right|^2 \le \left|\int \mathrm{d}x_o t_a^2(x_o)\right|^2 . \tag{8}$$

It is noted that the transmission functions $t_a(x_o)$ and $t_b(x_o)$ only take two values, 1 and 0, where 1 represents transparent, and 0 represents opaque. The front integral expressions are illustrated in Fig. 4.

Assume $t_a(x_o)$ is the transmission function defined in the range of $0 \sim x_2$, and $t_b(x_o)$ is the transmission function defined in the range of $x_1 \sim x_3$. Since the two objects are nonorthogonal, they should have the overlapping portion $x_1 \sim x_2$. And the integral function $\int \mathrm{d}x_o t_a(x_o) t_b(x_o)$ is equal to the area of the shaded part in Fig. 4(a). Likely, the value of $\int \mathrm{d}x_o t_a^2(x_o)$ is equal to the area of the shaded part in Fig. 4(b). Equation (8) can be rewritten as

$$x_2 \ge 2(x_2 - x_1). \tag{9}$$

Therefore, the object placed in the signal arm can be discriminated when the overlapping portion of the two objects in the set is less than one-second of the object placed in the signal arm.

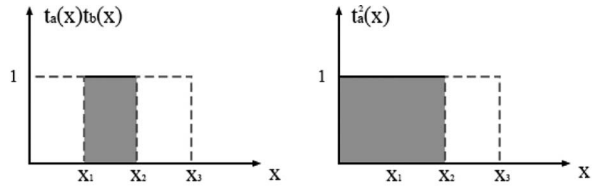

Fig. 4. Graph of the integral expressions. (a) Graphic form of $t_a(x_o)t_b(x_o)$. (b) Graphic form of $t_a^2(x_o)$.

More generally, when $x_2 \ge M(x_2 - x_1)$, the coincidence result recorded between detector D_1 and the detector that is corresponding to the object in the signal arm is at least M^2 times larger than the coincidence result recorded between detector D_1 and the detector that is not corresponding to the object in the signal arm.

And this is generalized to the condition of more objects in the set. Hence, nonorthogonal objects could be differentiated using ghost imaging.

3. NUMERICAL SIMULATIONS

In this section, we will present numerical simulations to verify the proposed method.

In the numerical simulation, we assume a laser with $LG_{l=0}$ mode pumping a BBO crystal to produce the entangled source $LG_{l=+1,-1}$, where the $l = 1$ mode light beam is in the signal arm, and the $l = -1$ mode light beam is in the idler arm. The simulation results for the identification of two nonorthogonal objects are shown in Fig. 5, where Fig. 5(a) shows the two pre-established amplitude objects with 4×4 pixels (far less than the beam radius). The object a is full filled with 1, and the object b is half filled with 1 and half with 0. Figure 5(b) shows the normalized coincidence results when the object a or object b is placed in the signal arm, respectively. When object a is placed in the signal arm, it is noted that the overlapping portion of objects a and b is just half of object a itself. According to the previous analysis, the normalized coincidence result between detector a and D_1 should be four times larger than the normalized coincidence result between detector b and D_1. It is easily found in the bar graph that the normalized coincidence result between

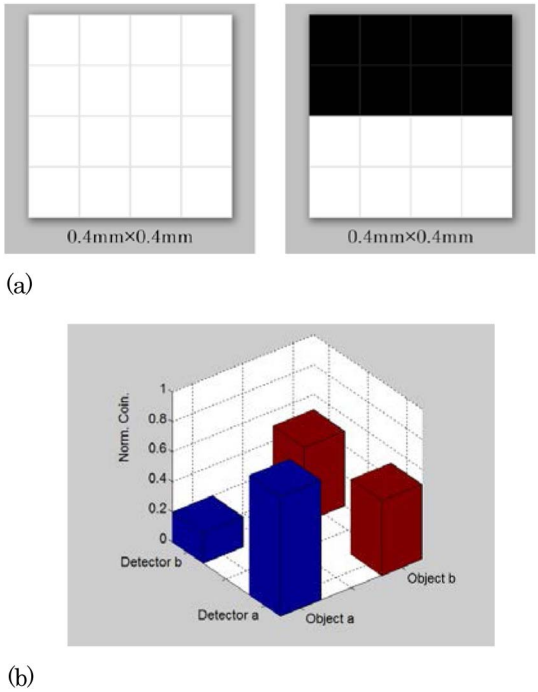

Fig. 5. Simulation results for the identification of two nonorthogonal objects. (a) Amplitude of object a and amplitude of object b. (b) Normalized coincidence results when object a or object b is placed in the signal arm.

detector a and D_1 is around 0.8, and the normalized coincidence result between detector b and D_1 is around 0.2. Thus, object a can be discriminated from object b by the difference between the two coincidence results. Similarly, when object b is placed in the signal arm, it is obviously noted that the overlapping portion of objects a and b is just the same as object b. So, the normalized coincidence result between D_1 and detector a should be the same as the one between D_1 and detector b. It is easily found in the bar graph that the normalized coincidence result between detector a and D_1 is around 0.5, and the normalized coincidence result between detector b and D_1 is around 0.5. Thus, this group of normalized coincidence results could not be used to make the identification.

It is shown that the two normalized coincidence results could be used to identify the object in the signal beam when the overlapping portion between the object is less than one-second of the object in signal beam, which is the bound for discriminating the nonorthogonal objects by the ghost imaging technique. This means that when the condition is not met, the two normalized coincidence results will not show enough difference to identify the unknown object.

Figure 6 shows the identification for a set of three objects using the proposed method, where Fig. 6(a) shows the three pre-established amplitude objects in 4×4 pixels. The middle 4×2 part of object a is filled with 1 and the others with 0, the top 4×2 part of object b is filled with 1 and the others with 0, and the bottom 4×2 part of object c is filled with 1 and the others with 0. Figure 6(b) shows the normalized coincidence results when object a, object b, or object c is placed in the signal arm, respectively.

It is also shown that the three normalized coincidences have enough difference to identify the unknown object, when the object under test (such as object a) has an overlapping portion with the other object (object b and object c) less than one-second of itself.

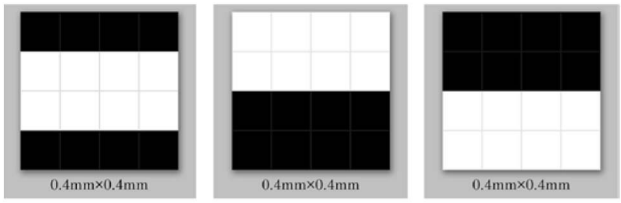

(a)

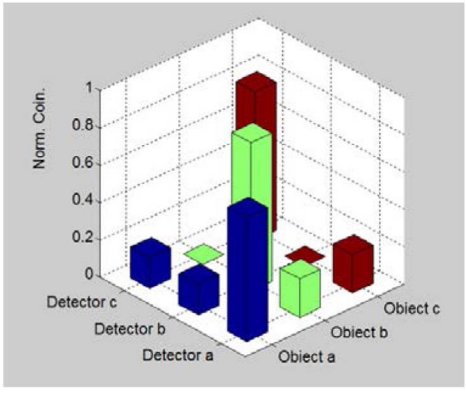

(b)

Fig. 6. Simulation results for the identification of three nonorthogonal objects. (a) Amplitude of object a, amplitude of object b, and amplitude of object c. (b) Normalized coincidence results when object a, object b, or object c is placed in the signal arm.

4. CONCLUSION

In this paper, we have presented a method to discriminate nonorthogonal objects based on ghost imaging. In the method, the unknown object is placed in the signal arm. A specific set of partially overlapping objects is required to build a multiple-exposure hologram first, and then the hologram is placed after the imaging position in the idler arm to diffract the idler photons into particular directions. By coincidence counting, the object in the signal arm can be identified with little photons and a short processing time. We have presented the bound of the overlapping portion of objects in a set for efficiently discriminating the object in the signal beam.

Numerical simulation results show that it is possible to identify nonorthogonal objects by the proposed identification method when the overlapping portion between any two objects is less than half of all the objects in the set.

ACKNOWLEDGMENT

The work was supported in part by the National Natural Science Foundation of China (Grant Nos. 61271238, 61475075), the Specialized Research Fund for the Doctoral Program of Higher Education of China (Grant No. 20123223110003), the University Natural Science Research Foundation of JiangSu Province (11KJA510002), and the open research fund of Key Lab of Broadband Wireless Communication and Sensor Network Technology, Ministry of Education (NYKL2015011).

REFERENCES

1. B. Moghaddam and A. Pentland, "Probabilistic visual learning for object representation," IEEE Trans. Pattern Anal. Mach. Intell. **19**, 696–710 (1997).
2. C. Stauffer and W. E. L. Grimson, "Learning patterns of activity using real-time tracking," IEEE Trans. Pattern Anal. Mach. Intell. **22**, 747–757 (2000).
3. H. Vogt, "Efficient object identification with passive RFID tags," in *Pervasive Computing* (Springer, 2002), pp. 98–113.
4. Y. Shih, "Quantum imaging," IEEE J. Sel. Top. Quantum Electron. **13**, 1016–1030 (2007).
5. J. H. Shapiro and R. W. Boyd, "The physics of ghost imaging," in *Quantum Information Processing* (Springer, 2012), pp. 1–45.
6. M. Malik, H. Shin, M. O'sullivan, P. Zerom, and R. W. Boyd, "Quantum ghost image identification with correlated photon pairs," Phys. Rev. Lett. **104**, 163602 (2010).
7. T. B. Pittman, Y. H. Shih, D. V. Strekalov, and A. V. Sergienko, "Optical imaging by means of two-photon quantum entanglement," Phys. Rev. A **52**, R3429–R3432 (1995).
8. R. S. Bennink, S. J. Bentley, and R. W. Boyd, "Two-photon coincidence imaging with a classical source," Phys. Rev. Lett. **89**, 113601 (2002).
9. A. Gatti, E. Brambilla, M. Bache, and L. A. Lugiato, "Ghost imaging with thermal light: comparing entanglement and classical correlation," Phys. Rev. Lett. **93**, 093602 (2004).
10. D. Cao, J. Xiong, and K. Wang, "Geometrical optics in correlated imaging systems," Phys. Rev. A **71**, 013801 (2005).
11. M. N. O'sullivan, K. W. C. Chan, and R. W. Boyd, "Comparison of the signal-to-noise characteristics of quantum versus thermal ghost imaging," Phys. Rev. A **82**, 053803 (2010).
12. C. Wang, D. Zhang, Y. Bai, and B. Chen, "Ghost imaging for a reflected object with a rough surface," Phys. Rev. A **82**, 063814 (2010).
13. F. Ferri, D. Magatti, L. A. Lugiato, and A. Gatti, "Differential ghost imaging," Phys. Rev. Lett. **104**, 253603 (2010).

14. Y. Zhou, J. Simon, J. Liu, and Y. Shih, "Third-order correlation function and ghost imaging of chaotic thermal light in the photon counting regime," Phys. Rev. A **81**, 043831 (2010).
15. G. Scarcelli, V. Berardi, and Y. Shih, "Can two-photon correlation of chaotic light be considered as correlation of intensity fluctuations?" Phys. Rev. Lett. **96**, 063602 (2006).
16. G. Scarcelli, V. Berardi, and Y. Shih, "Phase-conjugate mirror via two-photon thermal light imaging," Appl. Phys. Lett. **88**, 061106 (2006).
17. J. H. Shapiro, "Computational ghost imaging," Phys. Rev. A **78**, 061802 (2008).
18. Y. Bromberg and O. Katz, "Ghost imaging with a single detector," Phys. Rev. A **79**, 053840 (2009).